Journal of Molecular Catalysis A: Chemical 411 (2016) 247–256

Contents lists available at ScienceDirect

Journal of Molecular Catalysis A: Chemical

journal homepage: www.elsevier.com/locate/molcata

Preparation by sonophotodeposition method of bimetallic photocatalysts Pd–Cu/TiO_2 for sustainable gaseous selective oxidation of methanol to methyl formate

Paweł Lisowski*, Juan C. Colmenares*, Dariusz Łomot, Olga Chernyayeva, Dmytro Lisovytskiy

Institute of Physical Chemistry PAS, Kasprzaka 44/52, 01-224 Warsaw, Poland

ARTICLE INFO

Article history:
Received 5 October 2015
Received in revised form 27 October 2015
Accepted 29 October 2015
Available online 2 November 2015

Keywords:
Sonophotodeposition
Bimetallic
TiO_2
Sonication
Methanol photo-oxidation

ABSTRACT

It has been demonstrated that sonophotodeposition can be one choice as a green method to synthesize bimetallic supported photocatalysts with enhanced performance for selective oxidations. A series of Pd–Cu supported on Titania-P90 photocatalysts were successfully prepared using this innovative method of effective synergistic combination of sonication and light. In addition, our method does not require the use of strong chemical reduction agent and it is executed in a short time, room temperature and atmospheric pressure. The prepared materials were characterized by a number of techniques such as High-Resolution Transmission Electron Microscopy (HRTEM), DR UV–vis spectroscopy, X-ray Photoelectron Spectroscopy (XPS) and powder X-ray diffraction (XRD). Additionally, better bimetallic systems were obtained (methanol conversion >50% and selectivity to methyl formate >80%) by SonoPhotoDeposition (SPD) than in the case of the conventional photodeposition methodology. It has been discussed the possible reasons of the observed slight deactivation (8% after 2 h reaction test) of the best performing material in gas phase methanol selective photo-oxidation.

1. Introduction

Photocatalysts for selective oxidation must have, besides an appropriate location of the valence and conduction bands, a good absorption of photons, a long lifetime of the photoactivated species, a good adsorption of reactants and a relatively easy desorption of products. In this sense, structure, particle size and surface characteristics have been found to influence not only the activity, but also the selectivity of photocatalysed reactions [1–2]. One of the main advantages of using photocatalysis is the ability to operate reactions at room temperature, and this is especially relevant for selective oxidation reactions. Selective oxidation using photocatalysis potentially offers an alternative, safer and greener route for the synthesis of valuable chemicals [3–4].

In recent years, the development of novel environmental friendly and cost efficient methods for materials preparation that could replace the old ones is on demand. Unconventional and "soft" techniques such as sonication and photochemistry offer huge possibilities for the synthesis of a broad spectrum of nanostructured materials [5]. Ultrasonic treatment is one of the emerging tools that could be the alternative to thermal processing. It promotes the reaction under milder conditions where drastic conditions are required conventionally. Ultrasound functions by acoustic cavitation process that involves sequential formation, growth and collapse of microscopic vapor bubbles in the liquid. These localized hot spots have temperatures of roughly 5000 °C, pressures of about 500 atmospheres, and lifetimes of a few microseconds [6–7]. Suslick [8] performed much of the early work exploring the effects of acoustic cavitation on materials synthesis. The conditions produced during ultrasonic irradiation can be described as unusual, comparing to traditional energy sources, and they cannot be realized by other methods.

Photocatalyst deactivation phenomena are more predominant in gas phase than in aqueous phase, because in the latter the water molecules restore the surface hydroxylation and assist in the removal of the adsorbed species from the photocatalyst surface [9]. In gas phase reactions, intermediate species with slower kinetics and higher adsorption affinity than the target pollutant cause a deactivation that may sometimes be reversed by favouring their desorption or their photocatalytic degradation. Deactivation in the gas phase can differ in nature, and it depends on the type

* Corresponding author.
E-mail addresses: plisowski@ichf.edu.pl (P. Lisowski), jcarloscolmenares@ichf.edu.pl (J.C. Colmenares).

http://dx.doi.org/10.1016/j.molcata.2015.10.031
1381-1169/

of organic substrate being oxidized and also on the conditions of the photoprocess. An analysis of the open literature reveals that photocatalyst deactivation is generally found in continuous-flow photocatalytic reactors with a surface attached catalyst [10]. The catalyst may be deactivated either by formation of surface intermediates with higher adsorption ability than the target pollutant (reversible deactivation) or by sticky "heavy" products that are difficult to decompose or desorb (irreversible deactivation). Peral and Ollis [11] noted catalyst deactivation when photooxidizing 1-butanol and butyraldehyde in batch reactor. These authors proposed that the formation of strongly adsorbed butanoic acid in both cases was responsible for the catalyst deactivation. The deactivation of TiO_2 during the gas-phase photooxidation of trichloroethylene was reported by Larson and Falconer [12]. These researchers indicated that apparently strongly bound species, such as carbonates, accumulated on the surface deactivating the catalyst. Vorontsov et al. [13] investigated temperature deactivation of TiO_2 for acetone oxidation, and proposed that the accumulated surface products resulting from thermal oxidation of acetone caused deactivation. Méndez-Román and Cardona-Martıinez [14] studied the relationship between the formation of surface species and catalyst deactivation during the gas phase oxidation of toluene. Catalytic deactivation caused by byproducts was observed in the photocatalytic conversion of triethylamine over TiO_2 [15]. As pointed out by Sauer and Ollis [10], every single-pass catalytic process will eventually lead to the deactivation of the catalyst, often not observed in practice due to low levels of substrate or experiments carried out using short periods of time, or both. A better understanding of deactivation processes is essential for improving and optimizing process conditions, the catalysts themselves and for circumventing premature catalyst degradation in order to minimize additional costs.

Our systematic study of the photocatalytic oxidation of volatile organic compounds have led to receive highly active and selective photocatalysts prepared via SonoPhotodeposition (SPD) advanced methodology [16]. The advantages of SPD methodology over conventional methods include: preparation at room temperature and atmospheric pressure, no need to use reducing agents and very short reaction times. Furthermore, the physicochemical properties (high surface area and phase purity, particles with different sizes and shapes, uniform coating of nanoparticles on substrates, and many others) of the produced photocatalytic materials can be easily tuned by properly adjusting the parameters and conditions adopted in their preparation. In the present study, we modified the surface of commercial (Evonik) P90 TiO_2 with bimetallic Pd–Cu nanoparticles using SonoPhotoDeposition (SPD) advanced methodology. The modified Pd–Cu/TiO_2 photocatalysts were studied in the photocatalytic oxidation of methanol to methyl formate under UV illumination. The photocatalytic activity and selectivity of these materials were evaluated in our system for gas phase photocatalytic oxidation of alcohols [17]. Additionally, we provided some key insights in understanding the catalyst tendency to deactivate which we believe is due to the accumulation of "organic residues" on the surface of photocatalysts poisoning the Strong-Metal-Support-Interaction (SMSI) observed for the best performing photocatalytic system. To our best knowledge, this is the first time that a comprehensive study on this kind of systems has been reported.

2. Experimental

2.1. Photocatalysts preparation

Palladium (II) acetylacetonate (35% Pd, Acros), Copper(II) acetylacetonate (98% Cu, Acros) and commercial TiO_2 (AEROXIDE TiO_2 P90, Evonik Industries) were used as Pd, Cu precursors and TiO_2 as support. The detailed procedure was as follows: 0.1 g of oxalic acid and desired amount of precursors of palladium and copper were dissolved in 120 mL of H_2O:CH_3CN (30:70, v/v) and 0.5 g of TiO_2 was dispersed into this solution and pH was adjusted to ~2. The nominal palladium loading for all the bimetallic photocatalysts was designed as 1.0 wt.% (0.05 mmol) with different atom content Pd/Cu ratios of 9:1, 3:1 and 1:1. The batch photoreactor with such prepared mixture was placed into the ultrasonic bath (35 kHz, 560 W, Sonorex Digitec-RC, Bandelin) (Fig. 1). The suspension was first kept in the dark for 30 min to reach complete adsorption equilibrium. Sonophotodeposition was performed by illuminating the suspension for 60 min with a low pressure mercury lamp (6 W, λ_{max} = 254 nm) and with ultrasonic bath switched on. The average luminous intensity (~0.005 W/m^2) was determined by a radiometer Model HD 2302 (supplied by DELTA OHM, Italy) with UV-C laser power probe (220–280 nm). The synthesis reaction was carried out under argon flow (flow rate 70 mL min^{-1}) and thermostated at 20 °C. Then the product was recovered by slowly evaporation in rotary evaporator, dried at 110 °C for 10 h, and calcined at 300 °C for 4 h under air flow (flow rate 30 mL min^{-1}). The photocatalysts were labelled as 1 wt.%. Pd–Cu(9-1)/TiO_2 P90, 1 wt.%. Pd–Cu(3-1)/TiO_2 P90 and 1 wt.%. Pd–Cu(1-1)/TiO_2 P90. For comparative purposes, 1 wt.%. Pd/TiO_2 P90 and Cu(1)/TiO_2 P90 were prepared by sonophotodeposition method, and 1 wt.%. Pd–Cu(1-1)/TiO_2 P90 was synthesized by photodeposition (without ultrasounds). Unmodified TiO_2 P90 was chosen as reference material, without the addition of metal precursors.

2.2. Characterization methods

The specific surface area, pore volume, and average pore diameter were determined by N_2 physisorption using a Micromeritics ASAP 2020 automated system and the Brunauer–Emmet–Teller (BET)[18] and the Barret–Joyner–Halenda (BJH) methods [19]. Each photocatalyst was degassed under vacuum at $<1 \times 10^{-5}$ bar in the Micromeritics system at 300 °C for 4 h prior to N_2 physisorption.

Powder XRD measurements were performed using standard Bragg–Brentano configuration. This type of arrangement was provided using Siemens D5000 diffractometer (equipped with a horizontal goniometer) with $\theta-2\theta$ geometry and Ni filtered Cu Kα radiation, powered at 40 kV and 40 mA. Data were collected in the range of 2θ = 10–90° with step interval of 0.02° and counting time up to 5 s per step.

The average crystallite size (D in nm) was determined according to the Scherrer equation [20]:

$$D = \frac{k\lambda}{\beta\cos\theta} \quad (1)$$

where D is the average crystallite size of the catalyst (nm), λ is the wavelength of the Cu kλ X-ray radiation (λ = 0.154056 nm), k is a coefficient usually taken as 0.94, β is the full width at half maximum (FWHM) intensity of the peak observed at 2θ (radian), and θ is the diffraction angle. The phase contents of the samples can be estimated from the respective XRD peak intensities using the following equation [21]:

$$f_A = \frac{1}{1 + \frac{1}{K}\frac{I_R}{I_A}} \quad (2)$$

$$K = 0.79 f_A > 0.2$$

$$K = 0.68 f_A \leq 0.2$$

where:

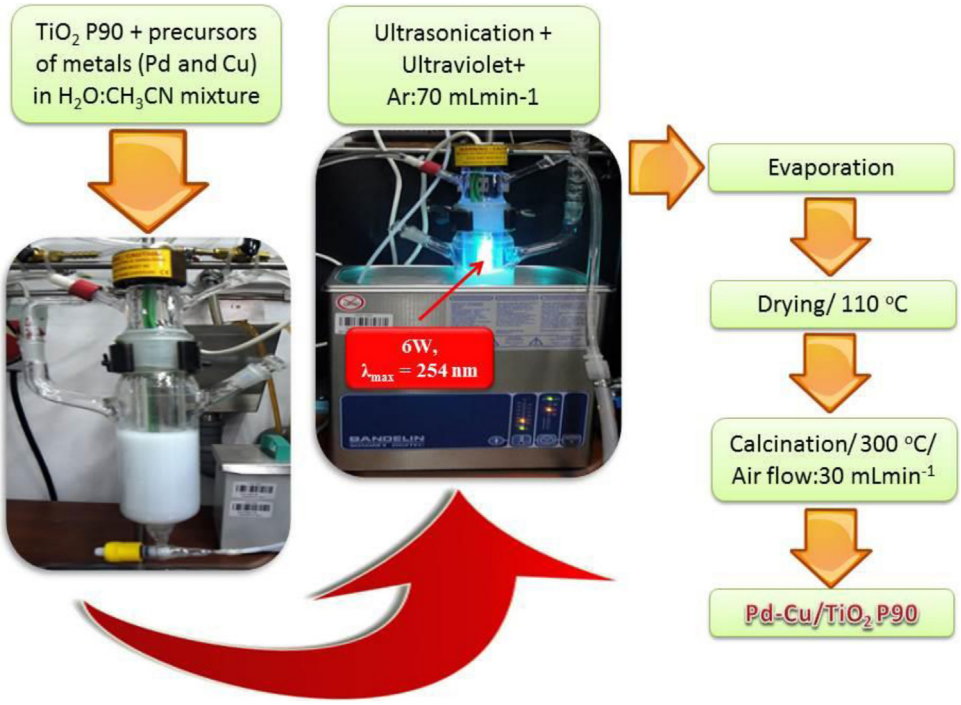

Fig. 1. SonoPhotodeposition advanced methodology for mono and bimetallic photocatalysts preparation.

f_A is the fraction of anatase phase in the powder, and I_A and I_R are the X-ray intensities of the anatase (1 0 1) and rutile (1 1 0) diffraction peaks, respectively.

HRTEM measurements were carried out using FEI TITAN Cubed electron microscope operated at an acceleration voltage of 300 keV and equipped with an energy dispersive X-ray (EDS) EDAX spectrometer. The samples were prepared by dispersing in pure alcohol using ultrasonic cleaner and putting a drop of this suspension on carbon films on copper grids and purified with plasma cleaner.

The XPS measurements were performed using a VG Scientific photoelectron spectrometer ESCALAB-210 using Al Kα radiation (1486.6 eV) from an X-ray source operating at 15 kV and 20 mA. Survey spectra were recorded for all the samples in the energy range from 0 to 1350 eV with 0.4 eV step. High resolution spectra were recorded with 0.1 eV step, 100 ms dwell time and 25 eV pass energy. Sixty degrees take-off angle was used in all measurements. The curve fitting was performed using the AVANTAGE software provided by Thermo Electron, which describes each component of the complex envelope as a Gaussian–Lorentzian sum function; a constant 0.3(±0.05) G/L ratio was used. The background was fitted using nonlinear Shirley model. Scofield sensivity factorsand measured transmission function were used for quantification. Aromatic carbon C 1s peak at 284.5 eV was used as reference of binding energy.

UV–vis Diffuse Reflectance spectroscopy was performed using a UV/VIS/NIR spectrophotometer Jasco V-570 equipped with an integrating sphere. The baseline was recorded using Spectralon™ (poly(tetrafluoroethylene)) as a reference material. Band-gaps values were calculated based on the Kubelka–Munk functions [22] $f(R)$, which are proportional to the absorption of radiation, by plotting $[f(R)\ h\nu)]^{1/2}$ against $h\nu$. The function $f(R)$ was calculated using Eq. (3):

$$f(R) = \frac{(1-R)^2}{2R} \tag{3}$$

Band gap values were obtained from the plot of the Kubelka–Munk function $[F(R_\infty)E]^{1/2}$ versus the energy of the absorbed light E. Regarding absorption threshold, it was determined according to the formula [23]:

$$\lambda = \frac{1240}{E_{gap}} \tag{4}$$

2.3. Photocatalytic activity measurements

The schematic representation of gas phase methanol photooxidation setup is given in Scheme 1 [17]. Methanol was introduced by bubbling the air (25 $cm^3\ min^{-1}$) through a glass saturator filled with methanol. The saturator was immersed in a thermostat kept at 0 °C. The gas flow rates were measured and controlled by mass flow controllers (supplied by Bronkhorst HI-TEC). The flow-type photoreactor was vertically enclosed by an aluminum foil cylindrical reflector (20 cm × 13 cm × 1 mm) to exclude any external light source and maximize light energy usage within the reactor. The photocatalyst bed height was 5 cm. The adsorption equilibrium reagent-photocatalyst was achieved in the dark after 2 h. The light source was a medium pressure 125 W mercury lamp (λ_{max} = 365 nm; supplied by Photochemical Reactors Ltd. Model RQ3010) built into a lamp housing and centered vertically in the reflector (2.5 cm between the lamp and photoreactor) and thermostated at 30 °C. The average luminous intensity (~260 mW/cm^2) was determined by a radiometer ILT 1400 (supplied by International Light Technologies, Inc., USA) with UV–vis laser power probe (250–675 nm). Reaction products were quantitatively analyzed by on-line gas chromatography (HP 5890 series II Hewlett Packard-USA equipped with a flame ionization detector (FID) and a methanizer model 510) (supplied by SRI INSTRUMENTS) and identified by gas chromatography coupled with mass spectrometry (HP-5 column GC (6890 Series)–MS(5973) Hewlett Packard equipped with FID and TCD Detectors).

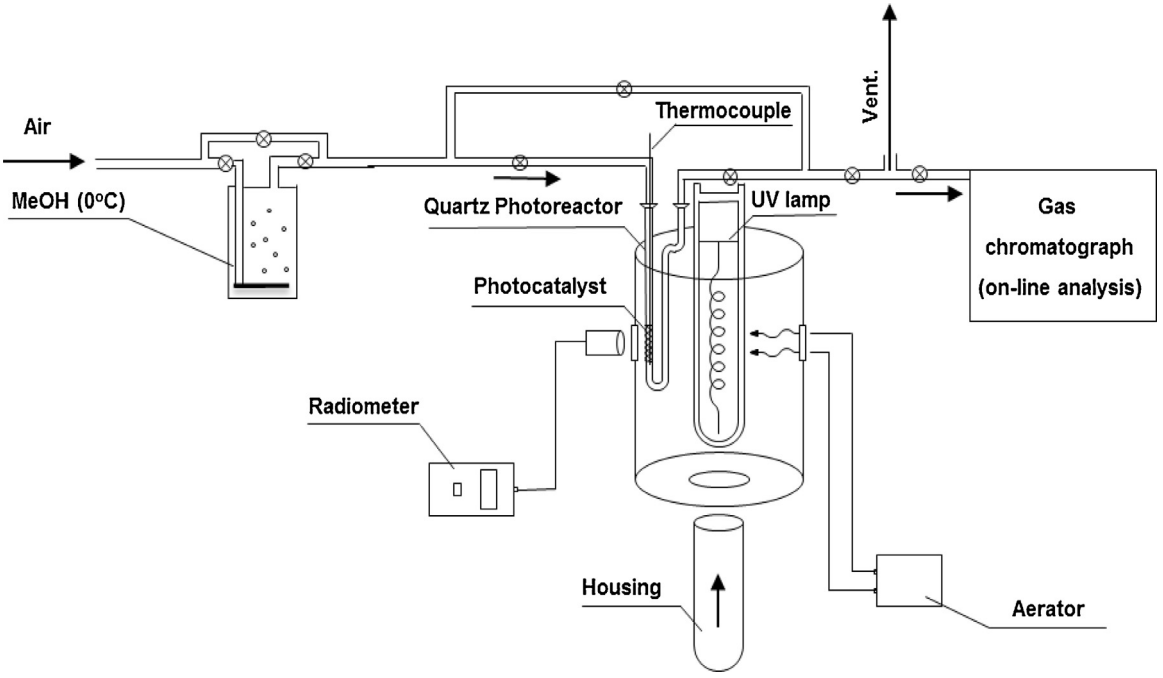

Scheme 1. Schematic representation of gas phase methanol photooxidation system.

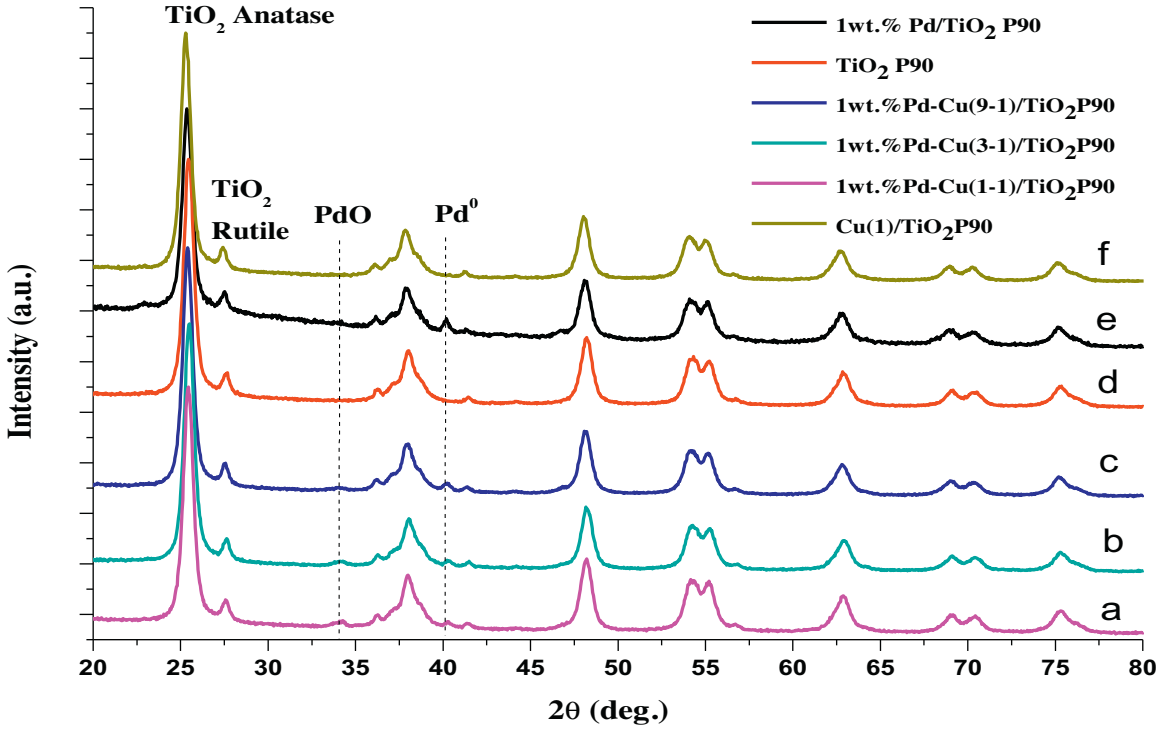

Fig. 2. XRD patterns of different photocatalysts: (a) 1 wt.% Pd–Cu(1-1)/TiO_2, (b) 1 wt.% Pd–Cu(3-1)/TiO_2, (c) 1 wt.% Pd–Cu(9-1)/TiO_2, (d) TiO_2 P90, (e) 1 wt.% Pd/TiO_2 P90 and (f) Cu(1)/TiO_2.

3. Results and discussion

3.1. Physico-chemical properties of the photocatalysts

In terms of photocatalyst specific surface areas (ca. 104 m^2g^{-1}), pore volume (ca. 0.47 mLg^{-1}), and pore diameter (ca. 15 nm, mesoporous), all materials showed very similar textural features. Determination of size and crystalline phase composition of the bimetallic photocatalysts were studied by XRD. Fig. 2 shows the diffraction peaks patterns of photocatalysts prepared by sonophotodeposition (SPD) method with different atom content Pd/Cu ratios of 9:1, 3:1 and 1:1. For comparison a pattern of monometallic 1 wt.% Pd/TiO_2 P90 photocatalysts and a pattern of commercial Evonik bare TiO_2 P90 were added. The average size of anatase and rutile crystallites for our photocatalysts, estimated by using the Scherrer equation, were about 13 and 25 nm, respectively (Table 1).

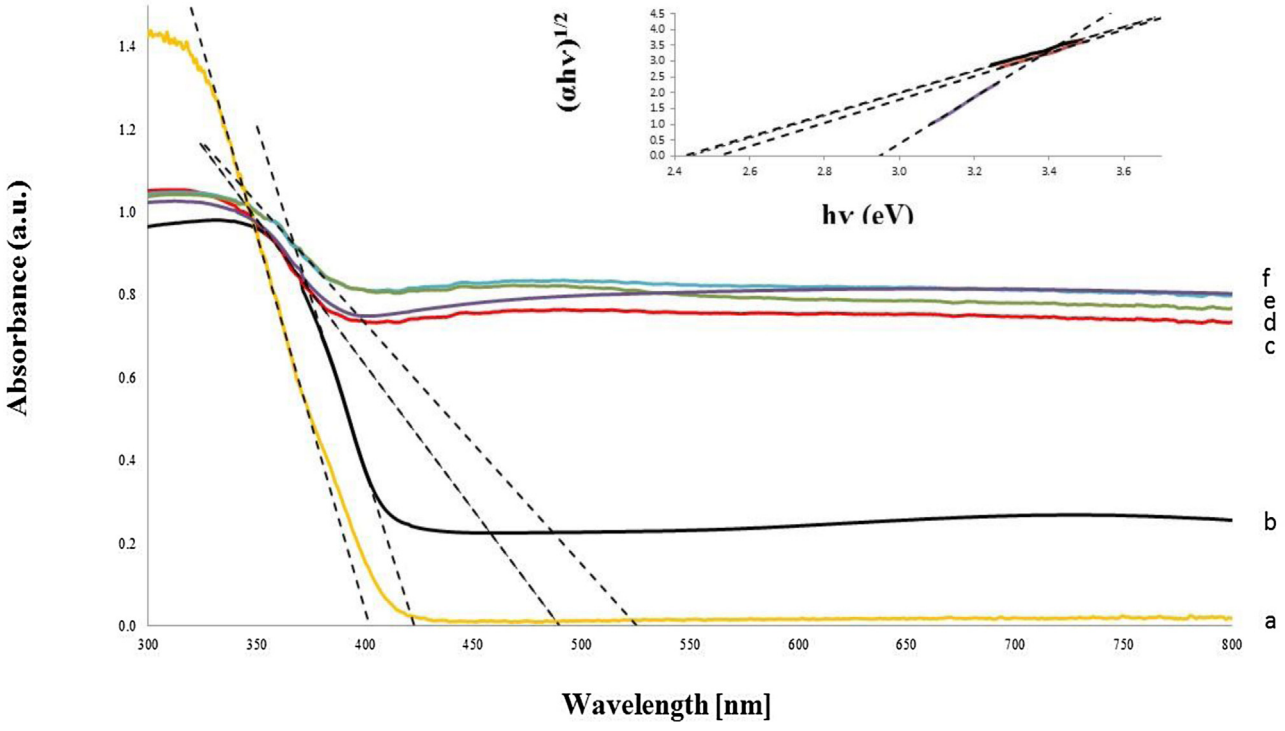

Fig. 3. DR UV–vis spectra of all tested photocatalysts: (a) TiO_2 P90, (b) Cu(1)/TiO_2, (c) 1 wt.% Pd–Cu(9-1)/TiO_2, (d) 1 wt.% Pd/TiO_2 P90, (e) 1 wt.% Pd–Cu(3-1)/TiO_2, and (f) 1 wt.% Pd–Cu(1-1)/TiO_2. Inset: photocatalyst band gap, E_g, calculations.

Table 1
Structural and optical properties of all tested photocatalysts prepared by the SPD method.

Photocatalyst	DR UV–vis		XRD				
	E_{gap} (eV)	Absorption threshold (nm)	Crystallite size (nm)		Crystal phase (%)[a]	Diameter of Pd^0 (nm)	Diameter of PdO (nm)
1 wt.%Pd Cu(9-1)/TiO_2 P90	2.53	490	14	25	A (55) R (45)	16	11
1 wt.%Pd-Cu(3-1)/ TiO_2 P90	2.40	516	13	27	A (57) R (43)	24	11
1 wt.%Pd-Cu(1-1)/ TiO_2 P90	2.40	516	13	26	A (59) R (41)	25	11
1 wt.%Pd/TiO_2 P90	2.51	493	12	26	A (74) R (26)	24	–
Cu(1)/TiO_2 P90	2.93	423	13	25	A (78) R (22)	–	–
TiO_2 P90	2.96	418	12	23	A (84) R (16)	–	–

[a] A stands for anatase and R for rutile.

Additionally, from the XRD patterns, peaks of palladium oxide phase (PdO: $2\theta = 34^\circ$) and metallic palladium ($2\theta = 40.1^\circ$) were detected for all bimetallic photocatalysts prepared by SPD method [24–26]. The crystallite sizes of palladium oxide in all bimetallic photocatalysts were approximately 11 nm and the crystallite sizes of palladium metal were two-fold larger (ca. 22 nm) for the photocatalysts prepared by SPD method (Table 1). Metallic Pd and palladium oxide PdO were obtained by SPD method, although, during the synthesis, calcination in air flow at 300 °C for 4 h was the last step. It is supposed that the role of sonication is crucial in the synthesis and for the explanation of our observations. Herein, sonochemically generated radicals, like $H^\bullet$ from sonolysis of water or some secondary radical species, are considered to act as reductants [5–8]. It is believed that these radicals can combine with oxygen atoms from the palladium (II) acetyloacetonate and therefore remove them from the organometallic precursor of palladium. At the same time, some part of metal ions can be reduced by these ultrasound-originated radicals and photo-electrons induced in the photodeposition process. Next, the material is subjected to calcination in air at 300 °C with the aim of removing the organic ligand of the palladium precursor. In the presence of carbon, remaining in the precursor, the oxygen from the air flow is consumed and palladium is reduced by the residual carbon. It was observed the XRD signal of PdO only for bimetallic systems (we do believe that the presence of copper could retard the total reduction of palladium). XRD patterns of photocatalysts do not show any clear signs of the presence of metallic Cu or CuO phases, probably due to the low amount (below the XRD detection limit) or the high dispersion of the copper loaded. The XRD spectra of bimetallic catalysts also do not show any signal that can be attributed to the Pd–Cu alloy phase.

The diffuse reflectance UV–vis spectra (Fig. 3) of synthesized samples showed the extension of the absorption band to the visible region (red shift) and a significant enhancement of light absorption at a wavelength of 418–516 nm. The results obtained indicated that visible-light absorption of TiO_2 P90 prepared by the SPD method was significantly improved by introducing Pd and Cu nanoparticles ($E_g \approx 2.4$ eV, absorption threshold $\lambda \approx 516$ nm; Table 1).

The absorption band edge is strongly related to the Cu and Pd nanoparticle size, shape, and Schottky barrier within the Pd–Cu/TiO_2 interfaces in the photocatalyst samples. For sample 1 wt.% Pd/TiO_2 P90, sharp absorbance edges occur at a wavelength of $\lambda \approx 493$ nm, and for Cu(1)/ TiO_2 P90 the absorbance edges occur at a wavelength of $\lambda \approx 423$ nm. The energy values (correlation coefficient $R^2 > 0.99$) corresponding to the forbidden energy (Eg) for each material were calculated and are reported in Table 1. The value for pure TiO_2 P90 and Cu(1)/TiO_2 were 2.96 eV and 2.93, respectively,

Table 2
XPS results for all tested photocatalysts prepared by the SPD method.

Photocatalyst		1 wt.% Pd–Cu(9-1)/TiO_2P90	1 wt.% Pd–Cu(3-1)/TiO_2P90	1 wt.% Pd–Cu(1-1)/TiO_2P90	1 wt.% Pd/TiO_2P90	Cu(1)/TiO_2P90	TiO_2P90 commercial
Cu 2p BE eV (at%)	Cu^0	932.1 (0.05)	932.2 (0.12)	932.4 (0.63)	–	932.4 (0.21)	–
Pd 3d BE eV (at%)	Pd^0	335.1 (0.03)	335.1 (0.04)	334.9 (0.09)	334.9 (0.06)	–	–
	PdO	336.2 (0.07)	336.3 (0.07)	336.3 (0.07)	–	–	–
Ti 2p BE eV (at%)	Ti^{4+}	458.6 (23.60)	458.8 (18.99)	458.8 (24.02)	458.7 (23.12)	458.7 (22.1)	458.8 (21.83)
	Ti^{3+}	–	–	456.8 (3.24)	–	456.5 (1.01)	–
C 1s BE eV (at%)	C—C	284.5 (11.28)	284.5 (15.31)	284.5 (5.47)	284.5 (5.27)	284.5 (9.16)	284.5 (6.32)
	C—OH	285.9 (2.66)	285.9 (5.84)	285.8 (1.80)	285.8 (4.00)	285.7 (3.93)	285.9 (4.29)
	C=O	287.4 (1.91)	287.5 (1.36)	287.4 (0.99)	287.4 (0.93)	287.4 (1.59)	287.4 (2.73)
	O=C—O	–	289.1 (0.93)	288.7 (0.94)	289.1 (1.33)	288.8 (0.86)	289.8 (1.36)
Pd/Ti atomic ratio		0.004	0.006	0.006	0.002	–	–
Cu/Ti atomic ratio		0.002	0.006	0.023	–	0.009	–

whereas the values for the materials containing Cu and Pd on the surface were between 2.40 and 2.53 eV; this indicates that there was a slight displacement of the Eg of TiO_2 to lower energy values when Cu and Pd particles were deposited on its surface. It has been reported by Kamat that contact of metal with the semiconductor indirectly influences the energetics and interfacial charge transfer processes in a favourable way [27]. Electron accumulation increases the Fermi level of the nanoparticle to more negative potentials and the resultant Fermi level of the composite shifts closer to the conduction band (CB) of the semiconductor. Therefore, the involved edge energy Eg in electron transfer from TiO_2 to the metallic nanoparticles is lower than that of bare TiO_2 and the addition of Pd and Cu leads to enhanced absorption of light in the visible region by TiO_2.

X-ray photoelectron spectroscopy (XPS) analyses were carried out to determine the chemical and electronic surface structure of formed nanoparticles and the valence states of the photocatalysts surface components. The binding energies (BEs) and atomic surface concentrations of all tested photocatalysts determined by XPS are given in Table 2. The Cu 2p, Pd 3d and Ti 2p binding energies (BEs) corresponding to oxidation states are listed in Table 2. In all samples the dominant peak of Ti 2p is located at 458.8 ± 0.08 eV and clearly corresponds to Ti^{4+} in TiO_2 structure [28–29]. The binding energy of Pd 3d in bimetallic photocatalysts were essentially similar, suggesting that electronic structure of the surface Pd atoms was not changed in the presence of surrounding neighbours. The presence of PdO on the surface can be ascribed to the coppers' retarding effect in the total palladium reduction process, and also due to the easy oxidation of Pd upon contact with air at room temperature as was observed by Herzing et al. [30] that some surface oxide layer of PdO persisted even after the reduction treatment. It should be noted that in all bimetallic photocatalysts studied, the binding energy (BE) signal from Cu^0 has shifted to higher (the higher the amount of copper the larger the shift) values which can be explained by a charge transfer from Cu^0 (presence of $Cu^{\sigma+}$) to titania support (SMSI effect), especially for the best performing photocatalyst 1 wt.% Pd–Cu(1-1)/TiO_2 P90 where the surface reduction of $Ti^{4+} \rightarrow Ti^{3+}$ is clearly seen (Table 2). The (Pd/Ti) atomic surface ratio is comparable in all bimetallic photocatalysts and a slight increases after the addition of copper is observed. This increases account a surface coverage by palladium species. On the other hand significant changes in the (Cu/Ti) was observed in all bimetallic photocatalysts confirming the surface enrichment in Cu due probably to the subsurface copper migration onto the titania surface (2.6-fold higher Cu/Ti atomic ration for 1 wt.% Pd–Cu(1-1)/TiO_2 P90 in comparison with Cu(1)/TiO_2P90, both with the same nominal amount of Cu). Additionally, following the comparison between these two photocatalysts, it was also observed approx. 3-fold higher concentration of $Cu^{\sigma+}$ and Ti^{3+} surface species for the best photocatalytically performing 1 wt.% Pd–Cu(1-1)/TiO_2 P90 material (Table 2, Figs. 6 and 8).

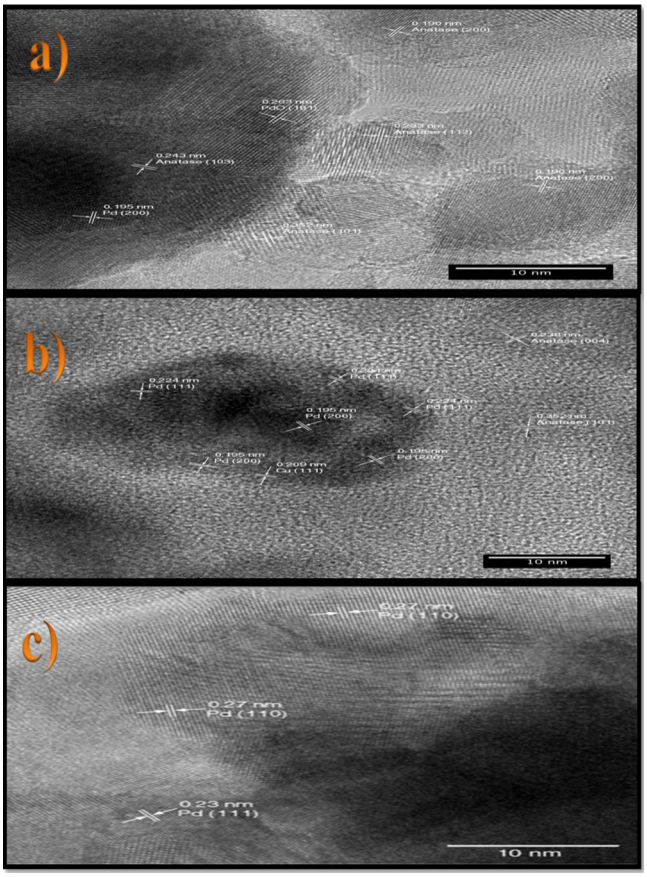

Fig. 4. HRTEM images of photocatalysts (a) 1 wt.% Pd–Cu(3-1)/TiO_2 P90, (b) 1 wt.% Pd–Cu(1-1)/TiO_2 P90 and (c) 1 wt.% Pd/TiO_2 P90.

Looking for more evidence regarding the nature of the deposited palladium and copper particles, high-resolution transmission electron microscopy (HRTEM) measurements were employed. Selected micrographs of Pd–Cu/TiO_2 and Pd/TiO_2 samples are shown in Fig. 4. As it can be observed in Fig. 4a–b in each system palladium and copper particles mostly form spherically shaped agglomerations with a diameter from dozen to ca. 100 nm. From the average particle size of TiO_2 P90, about 12 nm based on XRD measurements, the tendency to form aggregates is natural. All dark shadows in the HRTEM micrographs can be considered as metal-containing particles. Since both Pd and PdO were present in the sample according to XRD (copper was not detected probably due to the high dispersion), the darker areas are most likely attributable to metal presence, as an effect of denser material. It is interesting to note that all metal-containing species are always found in close contact especially for the best performing photocatalyst (Fig. 4b). However, it should

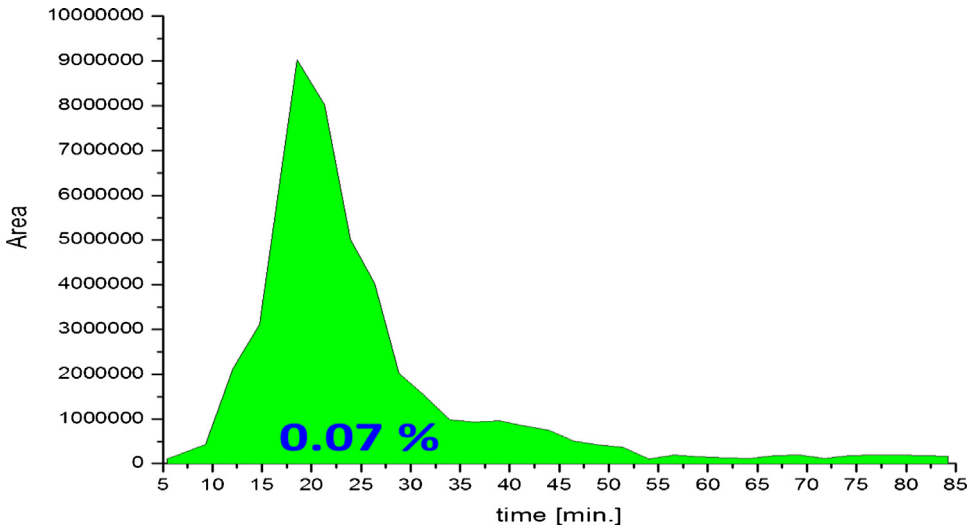

Fig. 5. TPO experiment of carbon deposited on 1 wt.% Pd–Cu(1-1)/ TiO_2P90 photocatalyst surface after 120 min of photocatalysis.

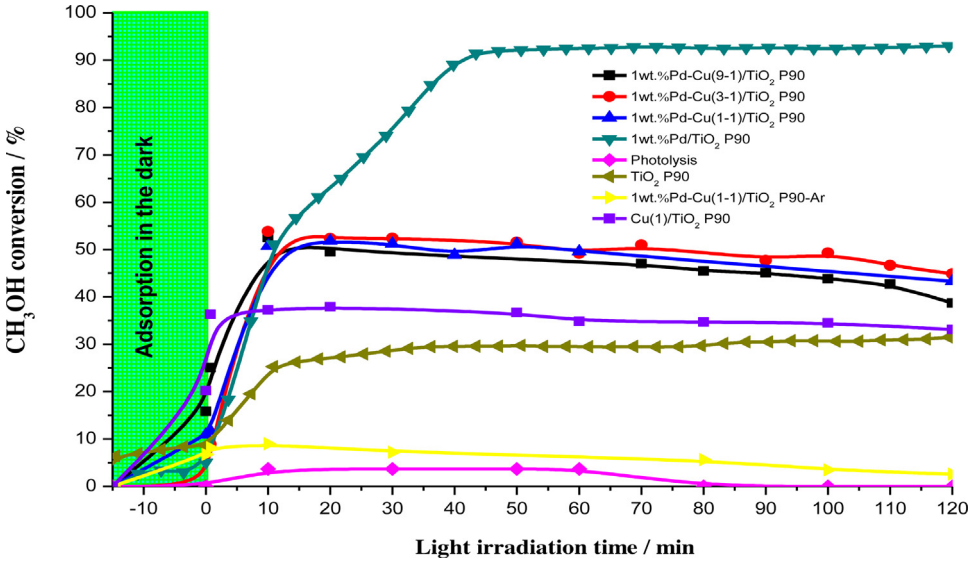

Fig. 6. Profiles of photocatalytic methanol conversion as a function of light irradiation time over all tested photocatalysts.

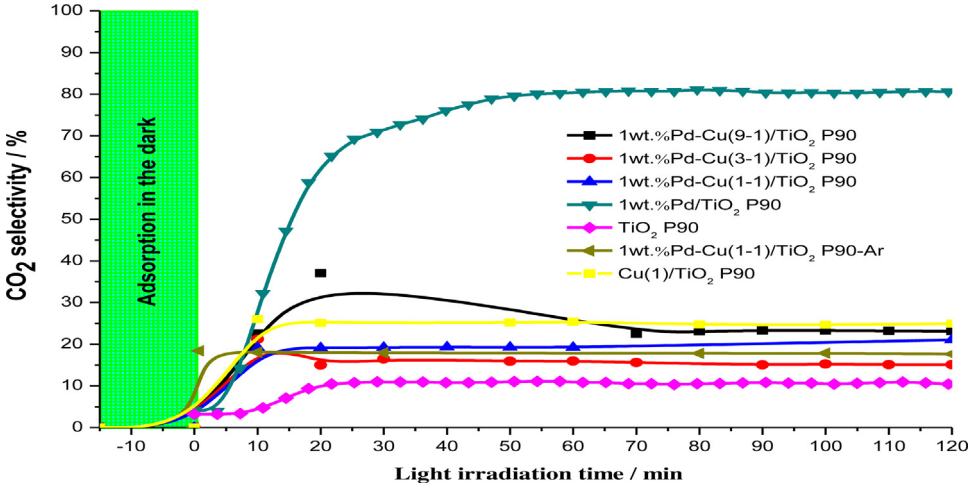

Fig. 7. Selectivity to carbon dioxide as a function of light irradiation time over all tested photocatalysts.

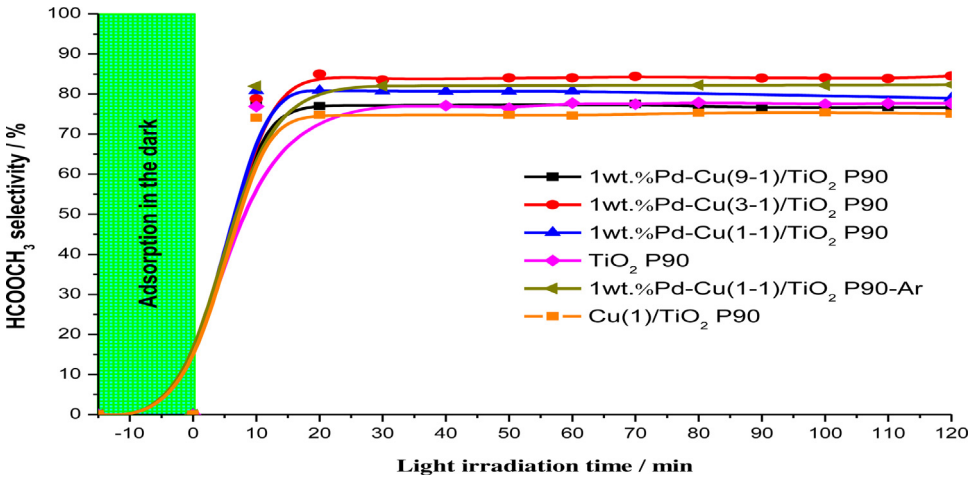

Fig. 8. Selectivity to methyl formate as a function of light irradiation time over all tested photocatalysts.

be pointed out that no core shell structure was obtained, but the domains are located next to each other as illustrated in Figure 4a–b.

3.2. Photocatalytic activity and stability

Photocatalytic oxidation of methanol in gas phase was chosen as the test reaction to evaluate photocatalytic properties of all prepared materials. After 2 h of light irradiation were identified CO_2 and methyl formate as the only two reaction products according to the following reactions (Eq. (1) and (2)):

$$2CH_3OH + 3O_2 \rightarrow 2CO_2 + 4H_20 \quad (1)$$

$$2CH_3OH + O_2 \rightarrow HCOOCH_3 + H_20 \quad (2)$$

Initially, three control experiments were applied: (1) photolysis upon UV illumination in the presence of methanol in the air flow and without photocatalyst, (2) photocatalytic methanol oxidation in the presence of the 1 wt.% Pd–Cu(1-1)/TiO_2 photocatalyst without oxygen (argon instead of air), and (3) the thermal effect (up to 100 °C) in the dark, in the presence of the photocatalyst and methanol in the air flow. Additionally, for the best performing photocatalyst (1 wt.% Pd–Cu(1-1)/TiO_2 P90), temperature-programmed oxidation (TPO) of coke deposited on its surface after 2 h of photocatalysis was conducted (Fig. 5).

In the photolysis experiment (absence of photocatalyst), very low conversion of methanol (<3%) was observed, thus confirming that the reaction is really enabled by a photocatalytic process. Moreover, the catalyst was not active under thermal conditions (up to 100 °C) in the dark. Therefore, the conclusion is that this reaction depends on the presence of both light and photocatalyst. In the absence of oxygen (air), 1 wt.%Pd–Cu(1-1)/TiO_2 P90 photocatalyst exhibited low methanol conversion (<10%) with slight deactivation and the highest selectivity to methyl formate (80%, Figs. 6 and 8). We believe that in the absence of oxygen (air), selective oxidation takes place through TiO_2 (in 1 wt.%Pd–Cu(1-1)/TiO_2 P90) lattice oxygen atoms and that oxygen (supplied in air flow) was needed only to replenish the produced oxygen vacancies on the TiO_2 lattice. When gas-phase oxygen was present, the oxidation rate of methanol was greatly improved (Fig. 6) suggesting the important role of adsorbed oxygen.

The TPO experiment was used to measure the amount of "organic residues" potentially remaining on the surface of the best performing photocatalyst (1 wt.% Pd–Cu(1-1)/TiO_2 P90) after the reaction. After 2 h of light irradiation, 1 wt.%Pd–Cu(1-1)/TiO_2P90 photocatalyst was heated first at 100 °C for 2 h in 25 mL min^{-1} of helium flow to remove all physisorbed reagents and products from the photocatalyst surface and then cooled down to room temperature from where a heating ramp rate of 10 °C min^{-1} was used up to 500 °C in 25 mL min^{-1} of air flow and GC on-line analysis of CO_2 (oxidation product) was monitored (Fig. 5). This TPO experiment showed the presence of carbon deposits on the surface of the photocatalysts in less than 0.07% of the total amount of methanol after 2 h of photocatalysis.

Fig. 6 displays the photocatalytic conversion of methanol over monometallic 1 wt.%Pd/TiO_2 P90 and bimetallic 1 wt.%Pd–Cu/TiO_2 P90 photocatalysts as a function of light irradiation time, together with TiO_2 P90 (Evonik) photocatalyst for comparison. It is clearly seen that modification of TiO_2 with palladium and copper applying sonophotodeposition method resulted in a great enhancement of photocatalytic activity and selectivity to methyl formate. Titania itself was active (ca. 33% methanol conversion, Fig. 6) only towards total oxidation of methanol to carbon dioxide under UV irradiation. It should be noted that the 1 wt.%Pd/TiO_2 P90 exhibited the highest methanol conversion among the all tested photocatalysts but without methyl formate production and with the highest grade of total mineralization (83%, Fig. 7) after 2 h of light irradiation. Among all tested materials the best selectivity (approx. 80%, Fig. 8) to methyl formate MF with good methanol conversion of 53% (this conversion was markedly increased at the initial stage of the reaction (first 15 min) and then slowly decreased with time (approx. 8% decrease) after 2 h of illumination, Fig. 6) was obtained for 1 wt.%Pd–Cu(1-1)/TiO_2P90 prepared by sonophotodeposition method as a function of light irradiation. It was also observed that photocatalysts containing Cu–Pd nanoparticles supported on TiO_2 P90 exhibit much lower mineralization rate to carbon dioxide under applied reaction conditions (Fig. 7). Furthermore, we obtained worse results for the 1 wt.% Pd–Cu(1-1)/TiO_2P90/PD (results not shown here) photocatalyst prepared by only the photodeposition method (methanol conversion of 28%, slowly decreased with time with approx. 5% deactivation after 2 h of illumination and selectivity to MF and CO_2 of 64% and 36%, respectively).

Since the activity tests described above were carried out with high purity gases, the inhibition by impurities in the gases is not the primary source for the deactivation. Nevertheless, numerous studies indicate that a certain degree of humidity, usually exceeding the amount produced by the oxidation of the organics, is necessary to maintain hydroxylation and to avoid the blockage of the TiO_2 surface by partially oxidized products [31–32]. Moreover, the hydrophilicity of the TiO_2 surface will influence the adsorption and desorption behavior of the reactants and products. Therefore the use of hydrocarbons with different molecular functionalities can help to get more insight into the charge transfer mechanisms. The

active site for a given product could be a certain atomic arrangement of metal atoms, the surface atom in a certain oxidation state, bimetallic surface site with a specific composition, or the interface between the metal nanoparticle and the oxide support. Under reaction conditions, active sites may reconstruct due to the light effect, or be blocked by strongly adsorbed intermediates. Our results potentially imply that the photocatalysts are deactivated by accumulation of surface species formed during the reaction [33]. Methanol for example will adsorb strongly to the surface and will form weaker adsorbed intermediates [34]. Decomposition of methanol proceeds via formation of methoxy (CH_3O) species, followed by either C—H or C—O bond scission. C—H bond scission leads to formaldehyde (CH_2O), formyl (CHO) and finally CO, followed by oxidation to CO_2 in the presence of adsorbed oxygen. O and C atomic co-adsorbates may play a critical role under reaction conditions. In the presence of oxygen, surface and bulk oxidation may occur, whereas carbon can accumulate on the surface, but also in the subsurface and bulk region. We believe (more research is needed to prove this) that these carbon species adsorb on [Pd—$Cu^{\sigma+} \leftrightarrow Ti^{3+}O_x$] active-selective site systematically poisoning the SMSI effect observed for our best photocatalyst. Under such conditions the contribution of C—O bond scission becomes stronger, leading to the formation of carbonaceous overlayers and to catalyst deactivation [35].

Nimlos et al. [36] reported that adsorbed maximum amount on TiO_2 and the adsorption equilibrium constant followed the sequence: acetic acid > ethanol > acetaldehyde. It indicated that carboxylic acid was strongly adsorbed onto the TiO_2 surface. Consequently, the deactivating species could be the carboxylic acid. The same decay of photocatalytic activity was observed when 1-propanol and propionaldehyde were photo-oxidized; the species responsible for the deactivation may be the same in both cases. It can be assumed that the deactivating species may be propionic acid, acetic acid or formic acid. The amount of intermediates was higher at lower mineralization extent, therefore more partial oxidized species were adsorbed on the catalyst surface to cause the loss of photocatalytic activity. Additionally, selectivity of heterogeneous photocatalytic reactions is ultimately determined by the relative concentrations of active sites for different reaction pathways. The deactivation may also to some extent be due to water inhibition generated in the mineralization reaction (production of CO_2 and H_2O).

The addition of copper improve the selectivity to methyl formate (>70%) in the monometallic Pd/TiO_2 system with slowly decreasing methanol conversion. In contrast, 1%Pd/TiO_2 P90 and TiO_2 P90 are non-active in the selective methanol oxidation to methyl formate but are active and selective to CO_2 formation (total mineralization). Such results suggest the advantages of the bimetallic Cu–Pd catalysts over the monometallic in the selective methanol conversion. The role of noble metals on semiconductor surfaces seems to be very well known. Many researchers claim that they act as efficient catalysts for electron transfer reactions and also decrease the recombination probability of photoholes with their counterparts (electrons) and therefore increase the fraction of photoholes available for oxidizing interfacial charge-transfer reactions [37]. In air atmosphere, the electron trapped by [Pd—$Cu^{\sigma+} \leftrightarrow Ti^{3+}O_x$] active-selective sites is transferred to O_2 and the superoxide anion is formed, $O_2^{\bullet -}$. After releasing the electron [Pd—$Cu^{\sigma+} \leftrightarrow Ti^{3+}O_x$] can trap another one and the whole process repeats leaving the photohole free and capable to oxidize selectively methanol. However, we should remember that the catalytic behavior of a bimetallic material may depend on both its electronic and geometric structure [38]. As one can see, the high selectivity to methyl formate depends highly on metals' loading, oxidation state of the metals and their interfacial behavior on titania surface. As was observed by XPS measurements, SMSI effect can have an important role in the selective oxidation of methanol. In such specific environment, the [Pd–$Cu^{\sigma+} \leftrightarrow Ti^{3+}O_x$] strong interactions are quite probable, especially after optimization of one of the most important parameters such as the appropriate metals' composition as it was observed for the best performing photocatalyst 1 wt.%Pd–Cu(1-1)/TiO_2 P90, but still this hypothesis needs more research to be totally proven.

4. Conclusions

Surface modification of TiO_2 with copper and palladium has been successfully carried out using sonophotodeposition method with TiO_2 P90 as support. Compared with the commercial reference, bare TiO_2 P90, UV–vis diffuse reflectance spectra indicate that the photoabsorption of Pd–Cu/TiO_2 photocatalysts is extended to the visible region. Bimetallic systems (especially 1 wt.%Pd–Cu(1-1) on TiO_2 P90) were nicely selective (approx. 80% of methyl formate) with good activity (53% conversion) and showing slow deactivation with time to approx. 8% conversion decrease after 2 h of illumination. As a matter of fact, the majority of the benefit comes from advantageous physicochemical properties of the Pd–Cu/TiO_2 P90 photocatalysts, in terms of size of its metal particles, their location relative to the support and their mobility, owing to an optimal extent of catalysts' strong metal-support interaction effect. This photocatalyst may also be slightly deactivated by accumulation of surface carbonaceous species formed during the reaction.

Sonophotodeposition method is a green methodology that can be used to prepare well-defined bimetallic surfaces on semiconductor supports with great promise for catalytic applications, in which selectivity can be tuned through adjustment of the surface composition.

Acknowledgements

This work was partially supported by the National Science Centre (NCN) in Poland within research project DEC-2011/01/B/ST5/03888. We would also like to thank the Institute of Physical Chemistry of PAS and the COST Association (Action FP1306) for supporting the dissemination of this work.

References

[1] Y. Qu, X. Duan, Chem. Soc. Rev. 42 (2013) 2568–2580.
[2] M.D. Hernandez-Alonso, F. Fresno, S. Suareza, J.M. Coronado, Energy. Environ. Sci. 2 (2009) 1231–1257.
[3] A. Fujishima, X. Zhang, D.A. Tryk, Surf. Sci. Rep. 63 (2008) 515–582.
[4] J.C. Colmenares, R. Luque, Chem. Soc. Rev. 43 (2014) 765.
[5] H. Xu, B.W. Zeiger, K.S. Suslick, Chem. Soc. Rev. 42 (2013) 2555.
[6] J.C. Colmenares, J. Nanosci. Nanotechnol. 13 (2013) 4787.
[7] J.H. Bang, K.S. Suslick, Adv. Mater. 22 (2010) 1039.
[8] K.S. Suslick, Science 247 (1990) 1439–1445.
[9] M. Lewandowski, D.F. Ollis, Appl. Catal. B Environ. 43 (2003) 309–327.
[10] M.L. Sauer, D.F. Ollis, J. Catal. 163 (1996) 215.
[11] J. Peral, D.F. Ollis, J. Catal. 136 (1992) 554.
[12] S.A. Larson, J.L. Falconer, Appl. Catal. B Environ. 4 (1994) 325.
[13] A.V. Vorontsov, E.N. Kurkin, E.N. Savinov, J. Catal. 186 (1999) 318–324.
[14] R. Méndez-Román, N. Cardona-Martinez, Catal. Today 40 (1998) 353.
[15] A. Huang, L. Cao, C. Jie, S. Franz-Josef, L.S. Steven, T.N. Obee, S.O. Hay, J.D. Freihaut, J. Catal. 188 (1999) 40.
[16] J.C. Colmenares, P. Lisowski, D. Łomot, O. Chernyayeva, D. Lisovytskiy, ChemSusChem 8 (2015) 1676–1685.
[17] J.C. Colmenares, P. Lisowski, Polish Patent Appl. (2013) P-405094.
[18] S. Brunauer, P.H. Emmett, E. Teller, J. Am. Chem. Soc. 60 (1938) 309–319.
[19] E.P. Barrett, L.G. Joyner, P.P. Halenda, J. Am. Chem. Soc. 73 (1951) 373–380.
[20] B.D. Cullity, S.R. Stock, Elements of X-ray Diffraction, 3rd ed., Prentice Hall Inc., Upper Saddle River, NJ, 2001.
[21] R.A. Spurr, H. Myers, Anal. Chem. 29 (1957) 760–762.
[22] S. Sakthivel, H. Kisch, Angew. Chem. Int. Ed. 42 (2003) 4908–4911.
[23] H.-S. Lee, C.-S. Woo, B.-K. Youn, S.-Y. Kim, S.-T. Oh, Y.-E. Sung, H.-I. Lee, Top. Catal. 35 (2005) 3–4.
[24] K. Mandal, D. Bhattacharjee, P.S. Roy, S.K. Bhattacharya, S. Dasgupta, Appl. Catal. A 492 (2015) 100–106.
[25] M.-S. Kim, S.-H. Chung, C.-J. Yoo, M.S. Lee, I.I.-H. Cho, D.-W. Lee, K.-Y. Lee, Appl. Catal. B Environ. 142–143 (2013) 354–361.

[26] O.S.G.P. Soares, M.F.R. Pereira, J.J.M. Órfão, J.L. Faria, C.G. Silva, Chem. Eng. J. 251 (2014) 123–130.
[27] P.V. Kamat, J. Phys. Chem. B 106 (2002) 7729–7744.
[28] C. Xua, Y. Liua, J. Wanga, H. Genga, H. Qiu, J. Power Sources 199 (2012) 124–131.
[29] J.F. Moulder, W.F. Stickle, P.E. Sobol, K.D. Bomben, Hand-book of X-ray Photoelectron Spectroscopy, in: J. Chastain (Ed.), PerkinElmer Corporation Physical Electronics Division, USA, 1992.
[30] A. Herzing, A.F. Carley, J.K. Edwards, G.J. Hutchings, C.J. Kiely, Chem. Mater. (2015) 20.
[31] M.M. Ameen, G.B. Raupp, J. Catal. 184 (1999) 112–122.
[32] A.J. Maira, K.L. Yeung, J. Soria, J.M. Coronado, C. Belver, C.Y. Lee, V. Augugliaro, Appl. Catal. B Environ. 29 (2001) 327–336.
[33] T.N. Obee, R.T. Brown, Environ. Sci. Technol. 29 (1995) 1223–1231.
[34] A.B. Anderson, H.A. Asiri, Phys. Chem. Chem. Phys. 16 (2014) 10587.
[35] M. Baumer, J. Libuda, K.M. Neyman, N. Rosch, G. Rupprechterz, H.-J. Freund, Phys. Chem. Chem. Phys. 9 (2007) 3541–3558.
[36] M.R. Nimlos, E.J. Wolfrum, M.L. Brewer, G. Bintner, Environ. Sci. Technol. 30 (1996) 3102–3110.
[37] A.A. Ismail, S.A. Al-Sayari, D.W. Bahnemann, Catal. Today 209 (2013) 2–7.
[38] B. Coq, F. Figueras, J. Mol. Catal. A: Chem. 173 (2001) 117–134.